Applied Catalysis B: Environmental 142–143 (2013) 752–760

Contents lists available at SciVerse ScienceDirect

Applied Catalysis B: Environmental

journal homepage: www.elsevier.com/locate/apcatb

The "cascade effect" of nano/micro hierarchical structure: A new concept for designing the high photoactivity materials – An example for TiO_2

Po-Chin Chen[a,b], Min-Chiao Tsai[a,c], Min-Han Yang[a], Ting-Ting Chen[a], Huang-Chin Chen[c], I.-Chun Chang[a], Yi-Chun Chang[b], Yu-Liang Chen[b], I.-Nan Lin[c], Hsin-Tien Chiu[b], Chi-Young Lee[a,*]

[a] Department of Materials Science and Engineering, National Tsing Hua University, Hsinchu 30013, Taiwan
[b] Department of Applied Chemistry, National Chiao Tung University, Hsinchu 30010, Taiwan
[c] Department of Physics, Tamkang University, New Taipei City 25137, Taiwan

ARTICLE INFO

Article history:
Received 27 March 2013
Received in revised form 30 May 2013
Accepted 31 May 2013
Available online 19 June 2013

Keywords:
Titanium dioxide
Hierarchical structure
Photocatalyst
Charge separation
Hetero-junction

ABSTRACT

The chrysanthemum-like TiO_2 (CT800) was synthesized. It exhibited excellent photoactivity, which greatly exceeded that of conventional P25. To discover the key factors that governed the photocatalytic properties, the specific reduction of Ag^+ ions was carried out and EPR spectra of CT800 were obtained. Both an HADDF image and EDX mapping indicated that the Ag^+ ions tended to be reduced close to the center of the micro matrix of CT800. Moreover, the EPR spectra strongly suggest that the excited electrons tended to migrate toward the center of the micro matrix, resulting from a multiple junction, cascade effect, which efficiently reduces the recombination of excited electrons and holes and greatly increases the photoactivity. Additionally, the special morphology of CT800 was responsible for the hot spots at the surface of nano sheets and then contributing to its outstanding photocatalytic activity. Furthermore, the unidirectional electron transfer, because of the cascade effect, by materials of different sizes provides a new avenue for the design of electronic and photoelectrochemical devices.

1. Introduction

Recently, nano/micro hierarchically structured materials have attracted considerable attention since their architectures combine the features of micro- and nano-scaled materials and exhibit unique properties that differ from those of the corresponding mono-morphological structures [1–3]. Their favorable performance in various applications, such as lithium-ion batteries [4], gas sensors [5], dye-sensitized solar cells (DSSCs) [6] and photocatalysts, have been reported upon [7]. To enhance the efficiency of photocatalysis, the key factors that govern photocatalysis attract the most attention by scientists. Numerous investigations have revealed that the high efficiency of a photocatalyst has several characters. (1) A high surface area can provide more active sites for the formation of photo-generated free radicals [8–10]. (2) A wide spectral absorption of light enables the use of considerable solar energy, yielding a higher photo-reaction rate. One means of using more solar energy is to reduce the band gap. Both doping with a small amount of impurity [11] and creating surface defects to form the sub-bands, can reduce the band gap of a material [12]. (3) Efficient charge separation by a hetero-junction can reduce the recombination rate of excited electrons and holes. Generally, a hetero-junction effect occurs between two materials [13,14] or polymorphs [15,16] that have different band gaps or energy states. The electrons tend to migrate to the lower energy states, and the holes migrate in the opposite direction, which strongly reduces the recombination of excited electrons and holes. Moreover, in our earlier study, a similar phenomenon was observed in a anatase TiO_2 single phase [17]. When the anatase titanium dioxides of different sizes were mixed, great photocatalytic performance was observed, resulting from the efficient charge separation, which was due to the hetero-junction between the different sized particles. As we know, the most effective charge separation system is the photosynthesis in nature. In plant cell, chloroplast is one of the major pigments performs photosynthesis efficiently. When light is absorbed, the excited electrons are formed and passed down to an electron transport chain, which consists of a series of electron acceptors with different energy states. This multiple electron transport process significantly reduces the electron-hole recombination making the photosynthesis efficient. (4) Hot spots on the surface of a material

* Corresponding author at: Department of Materials Science and Engineering, National Tsing Hua University, 101, Section 2, Kuang-Fu Road, Hsinchu 30013, Taiwan. Tel.: +886 3 5728692; fax: +886 3 5722366.
E-mail address: cylee@mx.nthu.edu.tw (C.-Y. Lee).

0926-3373/$ – see front matter © 2013 Elsevier B.V. All rights reserved.
http://dx.doi.org/10.1016/j.apcatb.2013.05.076

have been suggested to be photoactive sites [18–20]. Chen et al. demonstrated experimentally and numerically that highly photoactive sites were located at the interfaces among particles, and promoted efficient photocatalysis [18]. These key phenomena can be considered in the development of highly photoactive materials. TiO_2 is one of the most important functional materials because of its wide range of applications [21–31]. Recently, some forms of nano/micro hierarchically structured TiO_2 have been synthesized by various methods and have performed well in various applications [32–37], and especially as in photocatalysts [38,39]. This good performance must be accurately explained. Hence, this investigation seeks to elucidate the key causes of the good photoactivity of the nano/micro hierarchically structured TiO_2. In this investigation, a special "cascade effect" was observed in the nano/micro hierarchically structured TiO_2. The photo-excited electrons and holes were separated by a series of electron transfer between various energy states, reducing the recombination, which result in excellent photoactivity.

2. Experimental

2.1. Preparation of TiO_2

In this work, all chemicals were purchased from Aldrich Company and used directly without further purification. Chrysanthemum-like TiO_2 were synthesized from titanium isopropoxide (TTIP, 97%, Aldrich) and acetic acid (98–100%, Aldrich) by a simple solvothermal method. The details of the procedure can be found in our earlier work [4]. Once the reaction was complete, the solvent was removed by placing the products in a vacuum. The white powder, chrysanthemum-like titanate, was obtained (hereafter CT). The products were heated in air at 800 °C for 1 h at a temperature ramping rate of 1 °C per minute, and then cooled to room temperature (yielding a product that is referred to hereafter as CT800). CT800g was prepared by grinding CT800 in a mortar using a pestle by hand for 10 min.

2.2. Experiments on photocatalyst

The performances of TiO_2 (CT800, CT800g and P25) as a photocatalyst were studied. The samples were illuminated under an Xe lamp at an intensity of about 1 W cm^{-2}. Each powdered sample was placed in 25 mg L^{-1} methylene blue (MB) solution, stirred in the dark for 1 h, and then illuminated. During illumination, a trace amount of solution was removed every 5 min and centrifuged, before being filtered through a Millipore filter to separate out the TiO_2 particles. UV–vis spectra of the filtrates were obtained to determine the concentration of methylene blue.

2.3. Preparation of Ag@CT800

To determine the kinetics of photo-excited electrons in CT800, the powdered sample was suspended in $AgNO_{3(aq)}$ solution and illuminated under an Xe lamp. The concentration of $AgNO_{3(aq)}$ was 0.6 mM; the illumination period was 5 min. After illumination, the precipitate was collected using a centrifuge, washed several times with DI-water to remove the residual solvent $AgNO_{3(aq)}$ solution and then dried *in vacuo*. The product was subsequently examined by STEM (scanning transmission electron microscopy).

2.4. Characterization of materials

Scanning electron microscope (SEM) images were obtained using a JOEL-6500 field emission scanning electron microscope. Transmission electron microscopy (TEM) and STEM images were captured with a JOEL-2010 transmission electron microscope at an accelerating voltage of 200 kV, high-angle annular dark field (HADDF) images were acquired using an HAADF detector with an acceptance angle from 150 to 400 mrad. The structure of the powder was using a Brucker D8-advanced diffractometer (XRD) with Cu Kα radiation. Electron paramagnetic resonance (EPR) spectra were obtained using a Brucker E-580 Electron paramagnetic resonance spectrometer. The samples were placed in a Suprasil quartz glass tube with a diameter of 5 mm and then cooled to 10 K in 20 min, before being illuminated by an Xe lamp (120 W) for 20 min. Data were collected every 5 min at 10 K.

3. Results and discussion

3.1. Characterization of As-synthesized TiO_2

Fig. 1(a) and (b) presents the SEM image and XRD pattern of the chrysanthemum-like TiO_2 (CT800), respectively. The diameter of each particle is about 2 μm (Fig. 1(a)) and the XRD pattern of CT800 can be indexed to anatase (JCPDS, No. 21-1272). Fig. 1 (c) displays the TEM image of CT800, revealing a morphology that is consistent with the SEM image. Each particle is constructed from nano subulate sheets that grew radially from the center of the matrix. Additionally, the thickness of each nano subulate sheet gradually decreases. The thicknesses and grain sizes of zones 1, 2 and 3 from the tip of the sheet to the center of matrix follows the order zone 1 < zone 2 < zone 3. HRTEM was used to analyze the CT800 further. According to Fig. 1(d)–(f), the thicknesses in zones 1, 2 and 3 are approximately 5 nm, 15 nm and 30 nm, respectively. Numerous small grains formed in zone 1. In zones 2 and 3, the crystal grains are larger with better crystallinity. Additionally, it is worth mentioning that traces of immature particles were found in CT and CT800 (hereafter designated as immature CT and immature CT800, respectively), as shown in Fig. S1(a) and (b). Similar to mature particles, CT and CT800, the immature particles are also constructed by nano subulate sheets but the amounts of nano subulate sheet are much less than the mature particles. Therefore, the center of the chrysanthemum is exposed, and may be observed by SEM.

3.2. Photocatalytic test

The photoactivity of CT800 was investigated by studying the degradation of methylene blue (MB), using commercial TiO_2 (Degussa P25) as the reference. Fig. 2 depicts the photodegradation of MB by CT800 and P25. Obviously, CT800 exhibited higher photoactivity than P25: the k values of CT800 and P25 were 0.117 and 0.083, respectively. Recently, some reports have attributed the favorable photoactivity of P25 to its hetero-junction, which is formed as a synergistic effect of anatase and rutile [40–43]. Rutile can utilize not only UV light but also visible light, and can inject electrons into anatase while the holes remain in the rutile, resulting in charge separation. Hence, the recombination of excited electrons and holes is reduced, resulting in favorable performance of the photocatalyst. However, CT800 is composed of a single phase, anatase. The two-phase hetero-junction, comprising anatase and rutile, in P25 is not present in CT800. Therefore, the excellent photoactivity of CT800 must be attributed to other factors. In previous research, the high photoactivity of materials has usually been attributed to several factors, such as (1) a large surface area [8], (2) a wide spectral range of absorbed light [11,12], (3) efficient charge separation by the hetero-junction [13–16] and (4) hot spots on the surface of the material [18–20]. Comparing CT800 with P25 demonstrates that P25 has a higher specific surface area (52 cm^3 g^{-1}) than does CT800 (22 cm^3 g^{-1}) (Fig. S2). However, the spectral range of light absorbed by P25, which consists of mixed anatase and rutile phases, is wider than that absorbed by the single-phase CT800, because the

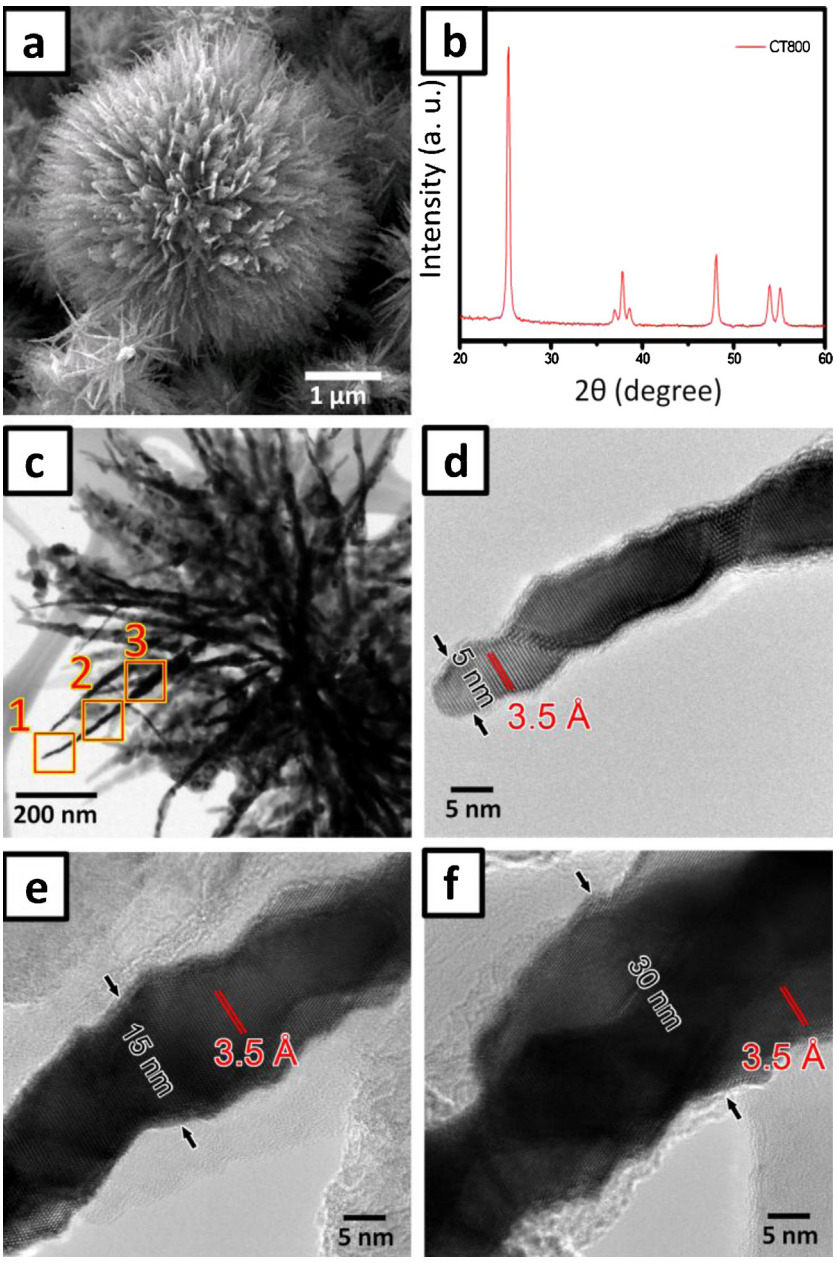

Fig. 1. (a) SEM image, (b) XRD pattern and (c) TEM image of CT800. (d), (e), and (f) HRTEM images that correspond to zones 1, 2 and 3 in (c).

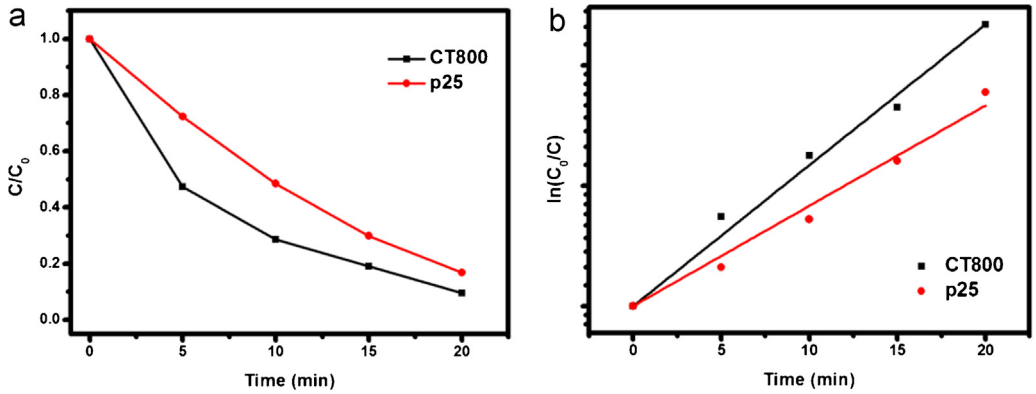

Fig. 2. (a) C/C_0 versus time for degradation of methylene blue (MB) and (b) $\ln(C_0/C)$ as a function time for CT800 and P25. The slopes of black and red lines are 0.11713 and 0.08339, respectively. C_0 and C denote initial concentrations at adsorption equilibrium and concentration of MB at various photodegradation times, respectively. (For interpretation of the references to color in this figure legend, the reader is referred to the web version of the article.)

Table 1
Small-particle size effects upon the BET surface area, wavelength at the band gap position, magnitude of blue shift of the band gap compared with bulk TiO_2, and quantum yields of the photocatalytic reactions of CH_3CCH with H_2O over anatase-type TiO_2, at 300 K [44].

Particle size (Å)	BET surface area ($m^2\ g^{-1}$)	Wavelength at band gap position (nm)	Magnitude of blue shift of band gap (eV)	Quantum yields[a] (%)
38	1068	371.5	0.156	7.18×10^{-2}
50	941	375	0.126	7.02×10^{-2}
65	609	380.5	0.079	8.80×10^{-2}
85	430	385	0.041	2.42×10^{-2}
110	312	387	0.024	2.26×10^{-2}
220	137	388	0.016	1.13×10^{-2}
530	26	389.9	0.000	0.264×10^{-2}

[a] Quantum yields were measured at 300 nm. Quantum yield = (number of photoformed products)/(number of incident photons).

band gap of rutile is smaller than that of anatase, expending the light absorption. Therefore, neither the first nor the second factor favors photocatalysis by CT800.

3.3. Cascade effect

The third factor, the hetero-junction, is associated with two materials or polymorphs, such as P25. Moreover, in our earlier investigation, a hetero-junction was found to be formed between particles of different sizes, even if they comprise only single phase of TiO_2 [17], because the band gaps in nano materials exceed those of bulk materials [44,45]. Anpo et al. also reported that both the band gap and photocatalysis quantum yields of anatase TiO_2 are increase with decreasing particle size of TiO_2 (Table 1). The large blue shift in the absorption spectra results from size-quantization effect [44–48]. These reports are consistent with our previous observations, the hetero-junction occurring between different sized particles of the same material. In the case of CT800, in the form of subulate sheets comprised chrysanthemums, the grains of the tips of subulate sheets are nano-sized, but the central parts of the chrysanthemums which consist of many large grains are micro-scaled. This variation in sizes of the grain in a particle causes variation in its band structure; the tips of sheets have higher energy state due to the larger band gap which is caused by the nano-sized grain. However, the grain sizes increased gradually along the direction toward the center of CT800, accompany with the decreasing in band gaps and quantum yield. Therefore, the central micro matrix has lower energy state. Hence, resulting in a series of electron transport from the tips of sheets to the central micro matrix, lead to the separation of electrons and holes, which greatly improves the photocatalytic properties. The electron transfer between grains in the sheet may be designated as a multiple junction, because of the grain size increased gradually from the tips of nano sheets to the central micro matrix, accompany with the gradationally decrease of energy state. The electrons migrate as a series of cascade toward the central micro matrix (Fig. 3). This phenomenon is analog to the electron transport chain in the photosynthesis. In additional, a gradient of electric potential resulting from the different amounts of excited electrons at the tip and the center of chrysanthemum also drive electrons from tip to center to generate "cascade effect". As previously reported [44], the quantum yield of the smaller nano grain is higher than that of the larger grain. Thus, during the illumination of CT800, the excited electrons at the tips of sheets are more than that at the central parts of the chrysanthemums. Accordingly, a gradient of electric potential was formed in between the tip and the central part. Subsequently, the excited electrons tend to migrate toward the central parts of the chrysanthemums, and the excited holes were move toward the different directions.

3.3.1. Examine the cascade effect by the specific reduction of Ag^+ ions

To examine the excited electrons move to the center part of CT 800 resulting in the great photocatalysis, the photo-reduction of $AgNO_3$ was studied using CT800 as the catalyst. CT800 was suspended in $AgNO_{3(aq)}$ solution and illuminated under an Xe lamp. Following illumination for 5 min, the precipitate was rinsed by DI water, yielding the brown product (Ag@CT800). Figs. 4(a) and (b) displays the STEM and HAADF images of Ag@CT800, respectively. The morphology of Ag@CT800 was similar to that of CT800, despite the presence of some small particles on it. Generally, in a large particle, the tip, edge and corner with high surface energy, usually lead to the nucleation on there [49–52]. However, the HAADF image

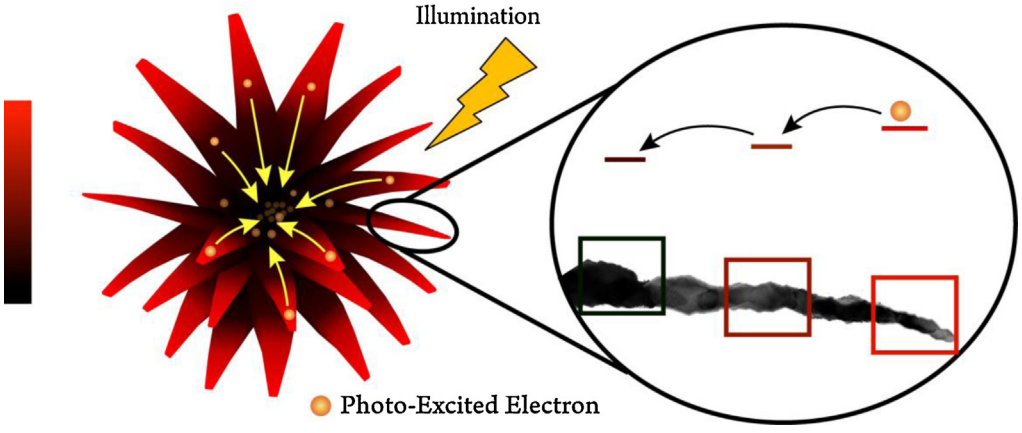

Fig. 3. "Cascade effect" of nano/micro hierarchically structured TiO_2. The bar showed in the left side represents the energy state, red and black colors represent high and low energy states, respectively. The colored chrysanthemum constructed by sheets which is illustrated at the center of the figure represents the energy state of the tips of nano sheets is higher than that of central micro matrix, owing to size effect, and the excited electrons tend to migrate toward the central micro matrix. The image of the sheet in the enlargement was extracted from TEM image. The excited electron at the tip (enclosed by red square) which has higher exciting energy state (red bar) tends to migrate to the lower excited energy state (black bar). (For interpretation of the references to color in this figure legend, the reader is referred to the web version of the article.)

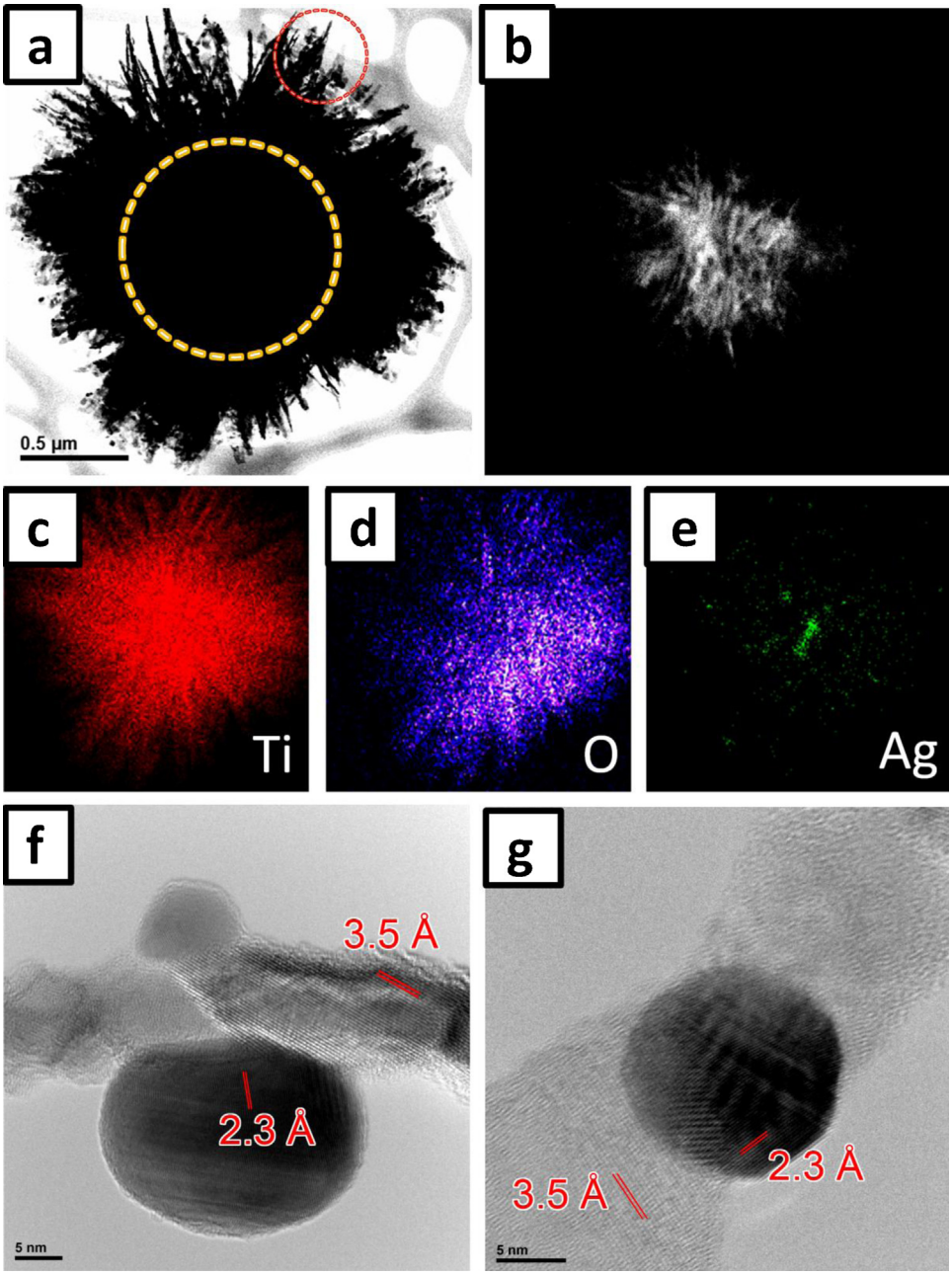

Fig. 4. The examination of migration behavior of the excited electrons by photo-reduction of Ag^+. (a) STEM image; (b) HAADF image of Ag@CT800; (c) EDX maps of Ti; (d) O and (e) Ag; (f) and (g) HRTEM images of Ag@CT800, revealing that Ag nanoparticles preferentially populate near the center and grain boundary of TiO_2 particle. The tip of nano sheets and the central micro matrix are enclosed by the red and orange rash circle, respectively.

reveals that Ag particles aggregated in the center of particles, indicating that the Ag^+ ions tended to be reduced near the center of the matrix. The central micro matrix in each particle seems to act as a "low-energy center" that attracts electrons from the tip of subulate sheets, resulting in the separation of excited electrons and holes. Additionally, EDX mapping was carried out to locate the reduced Ag particles. Fig. 4(c)–(e) shows the EDX signals that correspond to Ti, O and Ag, respectively. The center of the micro matrix was colonized by Ag particles, consistent with the HAADF image. A similar result was also obtained using an $AgNO_{3(aq)}$ solution with a high concentration and a longer period of illumination (Fig. S3). In addition, the different distribution of Ag particles precipitated on the tip and bottom part of the subulate sheets were further examined by photo-reduced Ag^+ using immature CT800 as catalyst. As shown in Figs. S1(c) and (d), a large Ag particle is clearly observed at the center by SEM, while a few very small particles at the tip of immature CT800, after 60 min illumination in 12 mM $AgNO_{3(aq)}$. The more Ag located at the center of the chrysanthemums was further substantiated by Ag distribution according to the EDX spectra (Fig. S4). Moreover, some reduced Ag particles were also located at the tips of the nano sheets. The TEM images in Figs. 4(f) and (g) reveals that some Ag particles are preferentially reduced at the grain boundaries of the nano sheets, suggesting that these boundaries serve as "hot spots", where electrons are likely to be trapped. Hence, the high photoactivity of CT800 can be explained by the efficient charge separation of electrons and holes due to the "cascade effect", and by the additional "hot spots" on the surface. In order to recognize the function of photo-excited hole, the photo-degradation experiments were executed with the addition of photo-excited hole scavenger, EtOH, which significantly decays the photoactivity of CT800 (Fig.

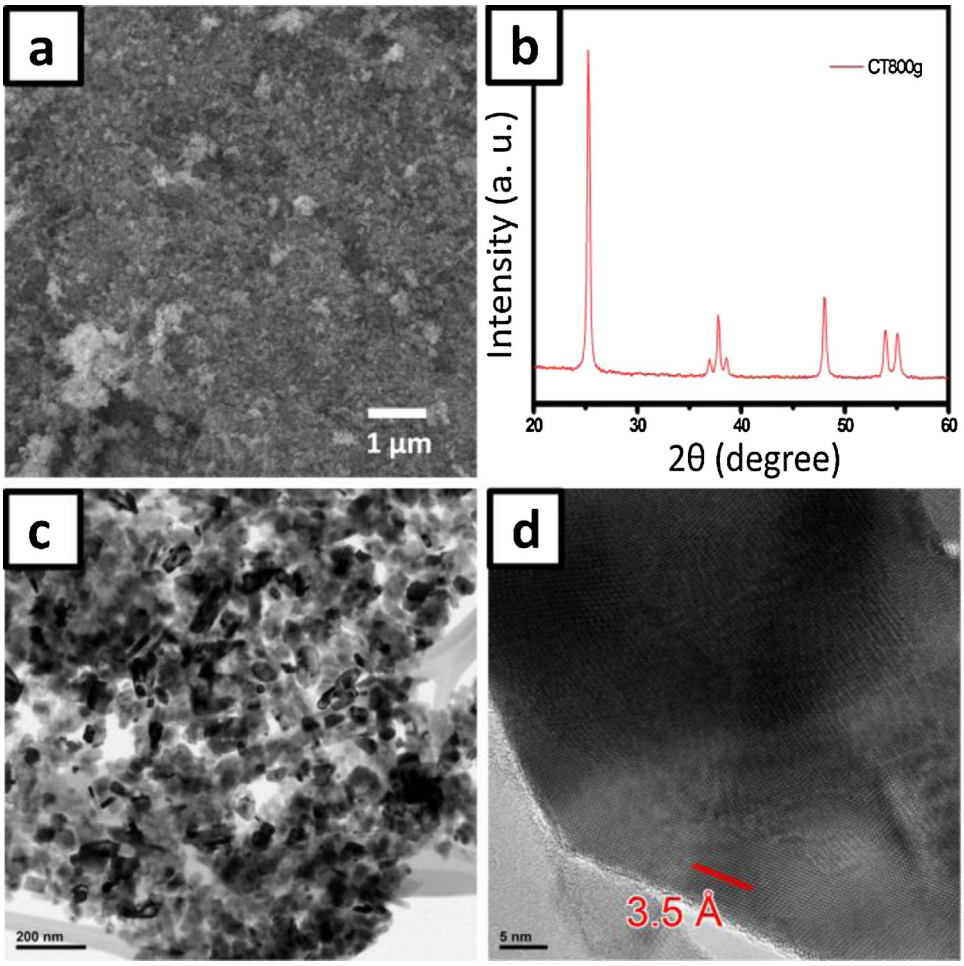

Fig. 5. (a) SEM image; (b) XRD pattern; (c) TEM image and (d) HRTEM image of CT800g.

S5). Thus, imply that the active excitons of the photo-degradation is hole.

3.3.2. *Examine the cascade effect by destroying the morphology of material*

To confirm further the "cascade effect", the morphology and photoactivity of ground CT800 (CT800g) were studied in detail. Fig. 5(a) and (c) presents the SEM and TEM images of ground CT800 (CT800g), respectively. The nano/micro hierarchical structure of CT800 was completely destroyed after grinding. The chrysanthemum-like morphology collapsed and became small fragments, causing the specific surface area of CT800g to be larger than that of CT800 (Fig. S2). The XRD pattern and HRTEM image reveal that the crystalline structure of CT800g is that of anatase (Fig. 5(c) and (d)). According to the XRD examinations and grain size estimation of CT800 and CT800g by Scherrer equation, both the grain sizes and crystallinity of CT800g are the same as those of CT800 (Fig. S6). Fig. 6 shows the photodegradation of MB by CT800 and CT800g. The CT800g had poorer photoactivity than CT800; the k value of CT800g was only 0.041, even though CT800g had larger

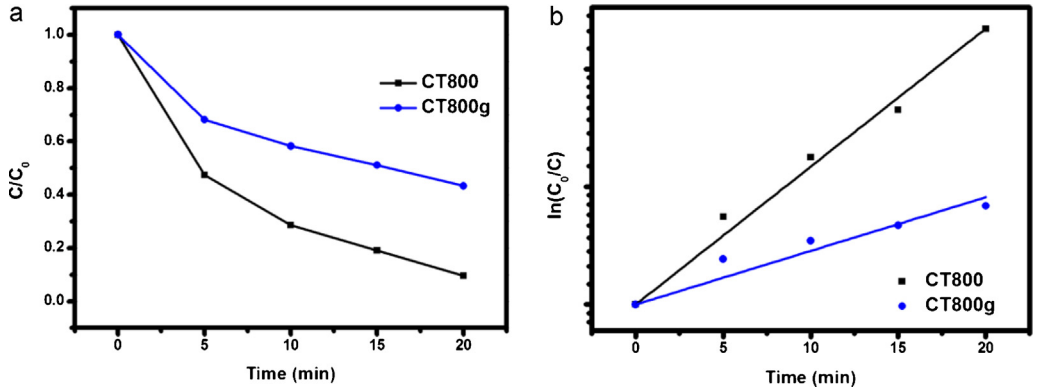

Fig. 6. (a) C/C_0 versus time for the degradation of methylene blue (MB) and (b) $\ln(C_0/C)$ as a function of time for CT800 and CT800g. The slopes of black and blue lines are 0.11713 and 0.04554, respectively. (For interpretation of the references to color in this figure legend, the reader is referred to the web version of the article.)

specific surface area. This result is not surprising, since CT800g did not have the nano/micro hierarchical structure, and so lacked the "cascade effect" and "hot spots" that promote photoactivity. The similar result was also observed when the fibrillar anatase TiO_2 was used as the active material of the photodegradation of MB (Fig. S7).

The light harvest of CT800 and CT800g were further studied by UV–vis spectra, as shown in Fig. 7. The additional absorption near the visible region of CT800g results from the small band gap of CT800g, reveals that some defects were generated on the surface by grinding [53]. The estimated band gaps of CT800g and CT800 are 3.19 and 3.25 eV, respectively. Increasing surface defects on CT800g slightly decrease its bandgap, resulting in the wider region of light absorption, which improve the light harvest. Moreover, after grinding, the surface area of CT800g is larger than that of CT800. According to these observations, CT800g is expected to exhibit better photocatalytic activity than that of CT800. However, the results revealed the reverse. Therefore, we proposed that the nano/micro hierarchical structure with "cascade effect" is one of the important factors that resulted in the great photocatalytic activity of CT800.

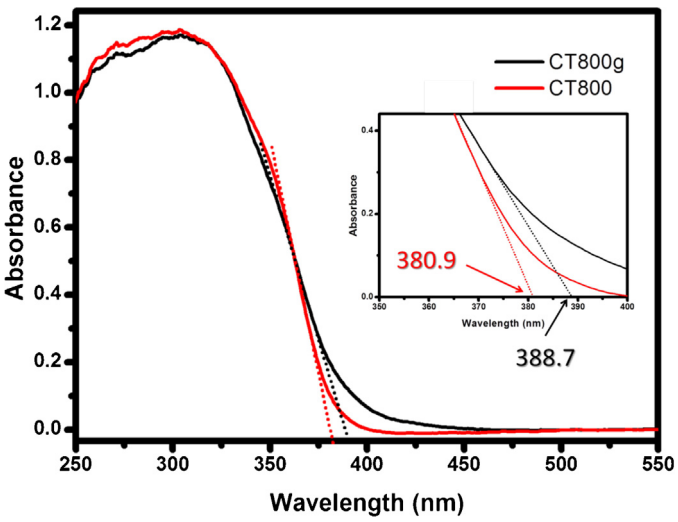

Fig. 7. UV-abs spectra of CT800 and CT800g powders.

3.3.3. *Examine the cascade effect by EPR*

The electron paramagnetic resonance (EPR) technique was adopted to investigate the electronic state of the photocatalysts under illumination. Fig. 8(a) and (b) presents the EPR spectrum of CT800 and CT800g, respectively. Under illumination, the intense signal at $g = 1.991$ can be identified as being associated with the trapped electrons in the lattice of anatase [54,55], and the broad

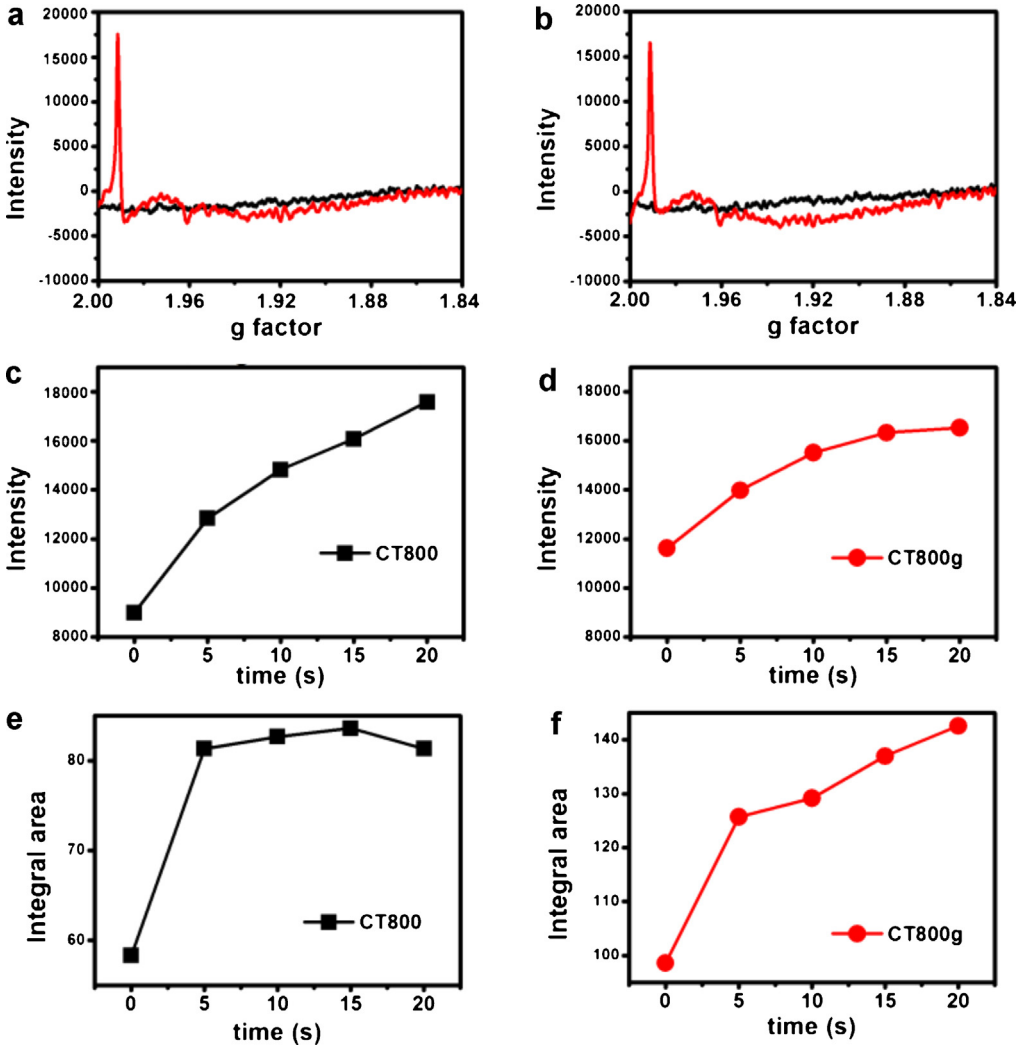

Fig. 8. EPR spectra of (a) CT800 and (b) CT800g; (c) and (d) EPR signal intensity that corresponds to lattice electron trapping sites in CT800 and CT800g, respectively; (e) and (f) integrated area under EPR signals that correspond to surface electron-trapping sites in CT800 and CT800g, respectively.

signal in the range $g = 1.86–1.95$ was attributable to the electrons that were trapped at the surface sites [56]. Such a broad signal indicates that electrons were trapped at various surface sites with various energy states [57]. Since the CT800 has a nano/micro hierarchical structure, we propose that the nano sheets contribute most of the surface electron trapping sites and the central micro matrix contribute most of the lattice electron trapping sites. To analyze further the kinetics of the excited electrons, Fig. 8(c) and (e) plots the variation of the intensity of the signals associated with the lattice and surface electrons, respectively, with time. Under illumination, the intensity of the signal from the lattice-trapped electrons of CT800 increased with the illumination time. However, the rate of increase decreased slowly for 15 min, after which the rate of increase increased slightly. The number of trapped electrons at the surface reached its maximum at 15 min, before declining. These observations strongly suggest that the flow of electrons was unidirectional, and the excited electrons that were generated at the tip of the nano sheets tended to move toward the center of the micro matrix from the tip of the nano sheets. In contrast, CT800g exhibited different features. The intensity of the trapped lattice electrons initially increased, saturating after 15 min (Fig. 8(d)), and the number of electrons trapped at the surface sites increased in proportion to the illumination time (Fig. 8(f)) because of the absence of the multiple junction. Moreover, in the EPR spectrum of CT800g, a broad signal that is related to the electrons that are trapped on the surface sites is also observed, it showed stronger intensity than CT800 because of the specific surface area of CT800g is larger than CT800.

4. Conclusion

In summary, TiO_2 (CT800) with a chrysanthemum-like morphology, constructed from nano subulate sheets that grew radially from the center of the matrix, was synthesized and exhibited outstanding photocatalytic performance. The excellent photoactivity of CT800 is attributed to (1) effective charge separation that is caused by the hopping of electrons from the tips of the nano subulate sheets to the central matrix of the particle by "cascade effect", and (2) the "hot spots" on the surface. The cascade effect of the nano/micro hierarchical structure was verified by the observation of the aggregation of electrons in the center of the chrysanthemum-like TiO_2 particle, as revealed by EPR and the specific reduction of Ag^+ ions. The photocatalytic reaction of TiO_2-related materials was investigated in detail. The results thus obtained provide in sight into the design of photoactive materials and help to explain the high photoactivity of nano/micro hierarchically structured materials. Furthermore, the unidirectional electron transfer, because of the cascade effect, by materials of different sizes provides a new avenue for the design of electronic and photoelectrochemical devices.

Acknowledgement

The authors would like to thank the National Science Council of the Republic of China, Taiwan, for financially supporting this research under contract no. NSC 100-2113-M-007-006-.

Appendix A. Supplementary data

Supplementary data associated with this article can be found, in the online version, at http://dx.doi.org/10.1016/j.apcatb.2013.05.076.

References

[1] J.S. Chen, Y.L. Tan, C.M. Li, Y.L. Cheah, D.Y. Luan, S. Madhavi, F.Y.C. Boey, L.A. Archer, X.W. Lou, Journal of the American Chemical Society 132 (2010) 6124–6130.
[2] D. Deng, M.G. Kim, J.Y. Lee, J. Cho, Energy & Environmental Science 2 (2009) 818–837.
[3] X.F. Gao, L. Jiang, Nature 432 (2004), 36-36.
[4] P.C. Chen, M.C. Tsai, H.C. Chen, I.N. Lin, H.S. Sheu, Y.S. Lin, J.G. Duh, H.T. Chiu, C.Y. Lee, Journal of Materials Chemistry 22 (2012) 5349–5355.
[5] H.G. Zhang, Q.S. Zhu, Y. Zhang, Y. Wang, L. Zhao, B. Yu, Advanced Functional Materials 17 (2007) 2766–2771.
[6] J.-Y. Liao, J.-W. He, H. Xu, D.-B. Kuang, C.-Y. Su, Journal of Materials Chemistry 22 (2012) 7910–7918.
[7] Y.F. Zhao, M. Wei, J. Lu, Z.L. Wang, X. Duan, Acs Nano 3 (2009) 4009–4016.
[8] F. Lu, W.P. Cai, Y.G. Zhang, Advanced Functional Materials 18 (2008) 1047–1056.
[9] T.J. Zhu, J. Li, Q.S. Wu, ACS Applied Materials & Interfaces 3 (2011) 3448–3453.
[10] W. Li, Y.H. Deng, Z.X. Wu, X.F. Qian, J.P. Yang, Y. Wang, D. Gu, F. Zhang, B. Tu, D.Y. Zhao, Journal of the American Chemical Society 133 (2011) 15830–15833.
[11] T. Ohno, T. Tsubota, M. Toyofuku, R. Inaba, Catalysis Letters 98 (2004) 255–258.
[12] M.Y. Xing, J.L. Zhang, F. Chen, B.Z. Tian, Chemical Communications 47 (2011) 4947–4949.
[13] V. Etacheri, M.K. Seery, S.J. Hinder, S.C. Pillai, Chemistry of Materials 22 (2010) 3843–3853.
[14] H.J. Huang, D.Z. Li, Q. Lin, W.J. Zhang, Y. Shao, Y.B. Chen, M. Sun, X.Z. Fu, Environmental Science & Technology 43 (2009) 4164–4168.
[15] Z. Ding, G.Q. Lu, P.F. Greenfield, Journal of Physical Chemistry B 104 (2000) 4815–4820.
[16] G.H. Tian, H.G. Fu, L.Q. Jing, B.F. Xin, K. Pan, Journal of Physical Chemistry C 112 (2008) 3083–3089.
[17] T.Y. Ke, C.Y. Lee, H.T. Chiu, Applied Catalysis A-General 381 (2010) 109–113.
[18] J.J. Chen, J.C.S. Wu, P.C. Wu, D.P. Tsai, Journal of Physical Chemistry C 115 (2011) 210–216.
[19] G.H. Li, S. Ciston, Z.V. Saponjic, L. Chen, N.M. Dimitrijevic, T. Rajh, K.A. Gray, Journal of Catalysis 253 (2008) 105–110.
[20] J.J. McDowell, J.I. McKelvey, L.A. Richard, J.T. Banks, Canadian Journal of Chemistry-Revue Canadienne De Chimie 86 (2008) 703–708.
[21] M.C. Tsai, J.C. Chang, H.S. Sheu, H.T. Chiu, C.Y. Lee, Chemistry of Materials 21 (2009) 499–505.
[22] D.V. Bavykin, J.M. Friedrich, F.C. Walsh, Advanced Materials 18 (2006) 2807–2824.
[23] T.Y. Ke, P.C. Chen, M.H. Yang, H.T. Chiu, C.Y. Lee, CrystEngComm 13 (2011) 5292–5295.
[24] M.C. Tsai, T.L. Tsai, C.T. Lin, R.J. Chung, H.S. Sheu, H.T. Chiu, C.Y. Lee, Journal of Physical Chemistry C 112 (2008) 2697–2702.
[25] J.M. Macak, H. Tsuchiya, A. Ghicov, K. Yasuda, R. Hahn, S. Bauer, P. Schmuki, Current Opinion in Solid State & Materials Science 11 (2007) 3–18.
[26] C.-T. Wang, C.-F. Yen, Journal of Sol-Gel Science and Technology 61 (2012) 83–89.
[27] M.C. Tsai, T.L. Tsai, D.B. Shieh, H.T. Chiu, C.Y. Lee, Analytical Chemistry 81 (2009) 7590–7596.
[28] M.-H. Yang, T.-T. Chen, Y.-S. Wang, H.-T. Chiu, C.-Y. Lee, Journal of Materials Chemistry 21 (2011) 18738–18743.
[29] G. Cernuto, N. Masciocchi, A. Cervellino, G.M. Colonna, A. Guagliardi, Journal of the American Chemical Society 133 (2011) 3114–3119.
[30] T.Y. Ke, C.W. Peng, C.Y. Lee, H.T. Chiu, H.S. Sheu, CrystEngComm 11 (2009) 1691–1695.
[31] M.C. Wu, J. Hiltunen, A. Sapi, A. Avila, W. Larsson, H.C. Liao, M. Huuhtanen, G. Toth, A. Shchukarev, N. Laufer, A. Kukovecz, Z. Konya, J.P. Mikkola, R. Keiski, W.F. Su, Y.F. Chen, H. Jantunen, P.M. Ajayan, R. Vajtai, K. Kordas, Acs Nano 5 (2011) 5025–5030.
[32] S. Ahmed, A. Du Pasquier, D.P. Birnie, T. Asefa III, ACS Applied Materials & Interfaces 3 (2011) 3002–3010.
[33] H. Bai, Z. Liu, D.D. Sun, Chemical Communications 46 (2010) 6542–6544.
[34] W. Hu, L. Li, W. Tong, G. Li, T. Yan, Journal of Materials Chemistry 20 (2010) 8659–8667.
[35] J.-Y. Liao, H.-P. Lin, H.-Y. Chen, D.-B. Kuang, C.-Y. Su, Journal of Materials Chemistry 22 (2012) 1627–1633.
[36] W.-P. Liao, J.-J. Wu, Journal of Materials Chemistry 21 (2011) 9255–9262.
[37] F. Sauvage, F. Di Fonzo, A.L. Bassi, C.S. Casari, V. Russo, G. Divitini, C. Ducati, C.E. Bottani, P. Comte, M. Graetzel, Nano Letters 10 (2010) 2562–2567.
[38] F. Di Fonzo, C.S. Casari, V. Russo, M.F. Brunella, A.L. Bassi, C.E. Bottani, Nanotechnology 20 (2009).
[39] L. Xiang, X. Zhao, J. Yin, B. Fan, Journal of Materials Science 47 (2012) 1436–1445.
[40] T. Ohno, K. Sarukawa, K. Tokieda, M. Matsumura, Journal of Catalysis 203 (2001) 82–86.
[41] T. Hirakawa, K. Yawata, Y. Nosaka, Applied Catalysis A-General 325 (2007) 105–111.
[42] Y.K. Kho, A. Iwase, W.Y. Teoh, L. Maedler, A. Kudo, R. Amal, Journal of Physical Chemistry C 114 (2010) 2821–2829.
[43] B. Sun, P.G. Smirniotis, Catalysis Today 88 (2003) 49–59.
[44] M. Anpo, T. Shima, S. Kodama, Y. Kubokawa, Journal of Physical Chemistry 91 (1987) 4305–4310.
[45] A.J. Nozik, F. Williams, M.T. Nenadovic, T. Rajh, O.I. Micic, Journal of Physical Chemistry 89 (1985) 397–399.
[46] L. Brus, Journal of Physical Chemistry 90 (1986) 2555–2560.
[47] L.E. Brus, Journal of Chemical Physics 79 (1983) 5566–5571.
[48] C.B. Almquist, P. Biswas, Journal of Catalysis 212 (2002) 145–156.
[49] M.T. Clavaguera-Mora, N. Clavaguera, D. Crespo, T. Pradell, Progress in Materials Science 47 (2002) 559–619.

[50] H. Cuppen, H. Meekes, W. Van Enckevort, E. Vlieg, Journal of Crystal Growth 286 (2006) 188–196.
[51] M.E. Glicksman, Principles of solidification: an introduction to modern casting and crystal growth concepts, Springer, 2010.
[52] P. Hartman, in: P. Hartman (Ed.), Crystal Growth: an Introduction, North-Holland, Amsterdam, 1973.
[53] S. Indris, R. Amade, P. Heitjans, M. Finger, A. Haeger, D. Hesse, W. Grunert, A. Borger, K.D. Becker, Journal of Physical Chemistry B 109 (2005) 23274–23278.
[54] I.R. Macdonald, S. Rhydderch, E. Holt, N. Grant, J.M.D. Storey, R.F. Howe, Catalysis Today 182 (2012) 39–45.
[55] O.I. Micic, Y.N. Zhang, K.R. Cromack, A.D. Trifunac, M.C. Thurnauer, Journal of Physical Chemistry 97 (1993) 7277–7283.
[56] D.C. Hurum, A.G. Agrios, K.A. Gray, T. Rajh, M.C. Thurnauer, Journal of Physical Chemistry B 107 (2003) 4545–4549.
[57] D.C. Hurum, K.A. Gray, T. Rajh, M.C. Thurnauer, Journal of Physical Chemistry B 109 (2005) 977–980.